Journal of Materials Chemistry B

ROYAL SOCIETY OF CHEMISTRY

PAPER

View Article Online
View Journal | View Issue

Cite this: J. Mater. Chem. B, 2025, 13, 15530

Fabrication of cell culture devices with integrated microfluidic networks *via* vat multimaterial 3D printing

Simona Villata, †[a] Chiara Santamaria,†[ab] Raquel Cue Lopez,[a] Giulio Galfrè,[c] Valentina Bertana,[c] Candido Fabrizio Pirri,[ad] Francesca Frascella *[a] and Ignazio Roppolo[a]

Over the past century, *in vitro* models such as cell cultures have been fundamental tools in the development of medicine and biology. However, these models are usually cultured in a static configuration that does not consider the complex conditions that occur *in vivo*, such as continuous nutrient and oxygen supply, and waste discharge. This study presents a bimaterial well plate called the BioFlowWellplate, which is characterised by wells that are connected through a microfluidic system. The device was fabricated using digital light processing (DLP), an additive manufacturing technique that allowed the complex geometry of the CAD model to be realised. A multimaterial approach was adopted for fabrication, with two different printable resins selected: PEGDA 250, which promotes cell adhesion and is transparent when printed in thin layers; and TEGORad®2800, which has great cytocompatibility and low drug retention. This has resulted in a biomedical device that enables users to save time and perform a more controlled procedure, while also allowing cells to be cultured in dynamic conditions for greater *in vivo* relevance in translational research. The presence of a microfluidic system connected to a pumping system not only allowed the automation of cell culture but also enhanced the relevance of an endothelium model cultured in both static and dynamic conditions. Finally, the BioFlowWellplate was successfully used for the dynamic perfusion of a 3D GelMA scaffold, paving the way for the dynamic culture of vascularised 3D *in vitro* models.

Received 8th July 2025,
Accepted 12th November 2025

DOI: 10.1039/d5tb01601k

rsc.li/materials-b

1. Introduction

In vitro models are widely used to improve understanding of the mechanisms underlying *in vivo* cell activity. They are now fundamental to drug testing and therapy screening, replacing conventional animal models.[1–4] These models can be cultured in static or dynamic systems.[5] The former involves growing cells on 2D surfaces or embedding them in matrices or scaffolds, without considering the complex growth conditions that occur *in vivo*, such as continuous nutrient and oxygen supply, and waste discharge.[6] Thus, static *in vitro* models do not accurately mimic the architecture and function of *in vivo* tissues. Developing a dynamic culture device could lead to *in vitro* models with greater *in vivo* relevance for translational research.[7–9] Unlike static cultures, dynamic cultures prevent rapid nutrient leakage and waste accumulation due to the small volume of media, which can be stressful and unphysiological for cultured cells. Conversely, dynamic cultures can facilitate the gradual consumption of nutrients and waste accumulation, leaving the cell culture medium to circulate.[10]

In this context, dynamic culture devices offer several advantages,[11] such as lower reagent volumes, a fast response time, low fabrication costs, high compactness and a high degree of scalability.[12] Additionally, these devices must have transparent parts to enable the overall condition of the cell culture to be monitored.

Several commercially available solutions successfully integrate cell culturing and microfluidics for such applications.[13,14] Nevertheless, there are still aspects to consider: the flow is often obtained through rocker-driven oscillation without replicating the continuous, monodirectional flow of the human circulatory system, which is critical for replicating *in vivo*-like conditions, particularly for applications involving shear-stress sensitive cell types or drug diffusion studies.[15] Moreover, as they are industrially designed, these commercially available devices

[a] Dipartimento di Scienza Applicata e Tecnologia, PolitoBIOMed Lab, Politecnico di Torino, Turin, 10129, Italy. E-mail: francesca.frascella@polito.it
[b] Department of Chemistry, Biology and Biotechnology, University of Perugia, Via Elce di Sotto 8, 06123 Perugia, Italy
[c] Chilab-ITEM, Politecnico di Torino, Chivasso, 10034, Italy
[d] Center for Sustainable Futures, Istituto Italiano di Tecnologia, Turin, 10144, Italy
† Equally contributed.

have defined shapes, volumes and connections, which does not allow for the necessary personalisation for experiment design.[16,17] More personalisable devices consist of microfluidic platforms, which are usually obtained by injection or replica moulding of polydimethylsiloxane (PDMS) using soft lithography masters.[18,19] Both techniques have disadvantages, as the manufacturing process involves multiple steps,[20] making them operator-dependent, time-consuming and wasteful of materials.[21] Furthermore, they both lack the ability to incorporate different materials in one device.

From a material perspective, PDMS has several advantageous properties that make it appealing for biological applications and microscopic observations,[22–24] but it has been criticised in drug testing due to its high absorption of small hydrophobic molecules, such as most drugs.[25,26] Consequently, the availability of the target molecule is lower than expected in drug testing.[25,27] In this context, a promising solution for fabricating devices for dynamic cell culture[28,29] is to use materials that have the same properties as PDMS[30,31] in terms of transparency, mechanical flexibility and cytocompatibility, but which can be 3D printed to overcome the aforementioned drawbacks. Vat polymerisation processes, such as digital light processing (DLP), are good candidates for this purpose. This additive manufacturing technology is based on photopolymerisation and enables the direct 3D printing of complex geometries with high precision. Since it employs liquid formulations, it also allows for the ease of designing materials, and it was selected as it offers higher resolution, smoother surfaces, and optical transparency compared to extrusion-based or inkjet multimaterial printing, which is critical for sealed microfluidic channels and cell imaging. Moreover, the cytocompatible resin chemistries available for vat polymerization made it particularly suited for biomedical applications.[20]

Based on these premises, this study presents a device for dynamic cell culture (BioFlowWellplate), developed using DLP fabrication technology. The well plate was fabricated using two different materials: a poly(ethylene glycol) diacrylate (PEGDA 250)-based resin was used for the bottom part since this material is cell-compatible, promoting good cellular seeding efficiency, and is transparent for microscopic analysis with suitable mechanical resistance.[32] An acrylate-PDMS (TEGORad® 2800)-based resin was used for the microfluidic structure to reproduce some standard PDMS device characteristics. Previous studies have also demonstrated that TEGORad can sustain cell growth without causing any genotoxic effects.[33] Moreover, flow experiments using a drug-like solution (Rhodamine 6G) showed that the retention of drugs in TEGORad is much lower than in PDMS.[33] Finally, the design of the device was tailored to enable cellular culture analysis using standard instrumentation, such as a plate reader and an inverted microscope.

The dynamic culture of an endothelium model is studied here as a target application of the BioFlowWellplate. The presence of endothelial cells (the main constituents of blood vessels) in human tissues has indeed been reported to play multiple roles, particularly in the form of a barrier and in cell-to-cell interactions during the immune response.[34] With regard to endothelial barrier function, it continuously permits the passage of solutes and small molecules, while limiting the extravasation of larger molecules and cells thanks to specialised cell-to-cell junctions (desmosomes, adherent junctions and gap junctions).[35] In this context, the endothelium plays a strategic role in drug delivery, both as an important therapeutic target in itself and as a barrier to reaching tissues beyond the vascular wall.[36] he main objective of this study was therefore to develop an advanced device for drug testing and therapy screening by hosting a dynamic endothelium model.

Finally, the proposed device was tested for the dynamic culture of 3D cellularised scaffolds, *i.e.* 3D *in vitro* models in which cells are embedded in different matrices.[37] One promising bioink for this purpose is methacrylated gelatin (GelMA),[38–43] a photo-crosslinkable hydrogel which is widely used as a matrix for cell culture in a variety of applications. In summary, the proposed BioFlowWellplate is versatile and can be used for a wide range of applications, supporting both 2D and 3D cell culturing in a dynamic manner. As it is based on 3D printing, it can also be adapted to the goals and design of different experimental setups.

To conclude, unlike existing dynamic well plates that rely on rocker-driven oscillatory flow, the BioFlowWellplate provides a continuous, monodirectional perfusion, reproducing physiological shear stress and nutrient gradients. Furthermore, in contrast to commercial systems with fixed geometries and materials, our platform combines optical transparency, cytocompatibility, and low drug absorption within a standard 96-well footprint. This integration is achieved through vat multimaterial 3D printing, which allows the seamless fabrication of complex, multi-material architectures not attainable by conventional molding or single-material 3D printing.

2. Materials and methods

2.1. Device design

BioFlowWellplate was designed (Fig. S1) and the CAD model was obtained with Solidworks SP05.1 following different experimental needs. The BioFlowWellplate was designed to match the dimensions and spacing of a standard commercial polystyrene 96-well plate (Greiner Bio-One), enabling compatibility with instrumentation calibrated for conventional plates (*e.g.*, plate readers). Each well has a diameter of 6.95 mm and a height of 10 mm, with a center-to-center spacing of 9 mm. The wells are arranged in three independent rows of four wells, with each row connected by a microfluidic channel (1 mm width, 1 mm height) to allow shared medium circulation within the row, while rows remain isolated from each other. Inlets and outlets (Ø 1 mm) at the channel ends enable connection to an external pumping system. The plate bottom was fabricated in PEGDA 250 to ensure cellular adhesion, transparency, and mechanical stability. Its thickness was 1.30 mm overall but reduced to 0.30 mm beneath each well to enhance optical transparency for microscopy. This design allows parallel dynamic culture experiments, preserves compatibility with standard analytical devices, and ensures that individual rows can be perfused with

independent media reservoirs. Regarding the microfluidic component, it was 3D printed employing TEGORad 2800 as resin, to have softer and deformable structure and easiness in removing the fluidics if necessary. Inlet and outlet were positioned at two different heights to facilitatefilling and fluxing of the plate. Moreover, the inner channels were designed with higher diameter than inlet and outlet to prevent clogging during the printing process. Indeed, this geometry improves washability and facilitates the removal of residual unreacted resin, ensuring unobstructed flow during perfusion.

2.2. Device support design

To ensure compatibility with instrumentation designed for standard commercial polystyrene cell culture well plates, (Greiner Bio-One) a support was designed (Fig. S2a). The support was milled from a Polymethylmethacrylate (PMMA) panel with holes aligned with the wells of BioFlowWellplate (Fig. S2a and b), to avoid interfering with the plate measurements or analysis (example in Fig. S2c represents compatibility with a plate reader) and can be coupled with the lid of a commercial polystyrene 96-well plate, if necessary (Fig. S2c).

2.3. Resin preparation, 3D printing and sterilization

In this work, two different formulations were used: a PEGDA 250-based for the bottom part and a TEGORad® 2800-based for the microfluidics. PEGDA 250 (*i.e.* poly(ethylenglycol)diacrylate, M_n 250) was purchased by Merck, while TEGORad® 2800 (or Acrylate PDMS) is an acrylate polydimethylsiloxane copolymer kindly supplied by Evonik Industries AG (Essen, Germany).

To prepare the PEGDA-based photocurable formulation, 1 wt% of photoinitiator (phenylbis(2,4,5-trimethylbenzoyl)-phosphine oxide, BAPO) and 0.1 wt% of radical scavenger (pentaerythritol tetrakis (2,5-di-*tert*-butyl-4-hydroxyhydrocinnamate, PT)) were added. A dark falcon was used to prevent polymerization of the formulation due to visible light. The resulting solution was then sonicated for 5 minutes to achieve homogeneity. Once completed, the resin was directly used for the 3D printing process.

To prepare the TEGORad-base photocurable formulation, 0.8 wt% of BAPO dispersed in 2-hydroxy-2 methylpropiophenone (Merck), weight ratio 1 : 4 was added. Also, Disperse Red 1 methacrylate (Merck) was used as a dye. The dye was added to enhance the resolution during printing. In this technique, light penetration depth can blur fine geometries, and the dye can absorb excess light, limiting over-curing and improving the accuracy of printed structures. Since this dye is not directly soluble in TEGORad® 2800, it was dissolved in Methyl Methacrylate (Merck), with a 1 : 50 weight ratio. A dark falcon was used to prevent polymerization of the formulation due to visible light. The mixture was initially stirred for 15 minutes and then sonicated for 5 minutes at 35 °C. For both formulations, the percentages of the different ingredients are to be considered with respect to resin (*i.e.* phr). Formulations are summarized in Tables S1 and S2.

A DLP printer (Asiga MAX) with a light source of 405 nm was used to print the bimaterial BioFlowWellplate. The device was printed by setting specific parameters: the thickness of each layer was the same for both formulations, set at 50 μm, and the light intensity was also the same, set at 22.19 mW cm^{-2}. For the different structures of the device (*e.g.* channels, base, walls), the exposure times were optimized separately (see Table S3). After 3D printing, samples were subjected to a post-curing treatment under UV light (intensity 50 mW cm^{-2}) to complete the crosslinking, 5 minutes each side. Next, with the goal to wash properly the BioFlowWellplate to avoid the release of cytotoxic substances, the sample was placed inside a beaker filled with ethanol. Two ethanol incubations of 30 min were followed by an overnight in ethanol. Afterwards, the BioFlowWellplate was placed in a Phosphate Buffered Saline (PBS, Merck) bath overnight and subsequently exposed to UV light in a biological hood for 30 minutes each side to obtain sterilization of the device.

2.4. Scanner 3D

3D Scanner 3Shape E3 was used to quantitative evaluate the print resolution of the scan theBioFlowWellplate.

2.5. Fluidic simulations and tests

To perform Fluidic simulations, COMSOL Multiphysics 6.1 software[49] was used. The CAD model file (.STEP) created for the plate production was imported as input geometry (Fig. S3a). Then the plate was simplified: only one line (*i.e.* three cascade wells) was considered for simulation and the symmetry across the longitudinal direction of the channel was exploited to further reduce the complexity of the problem. The fluid volume was added directly in the COMSOL Geometry interface, and the results are shown in Fig. S3b.

Then materials were assigned to domains. In particular, the liquid was considered as the COMSOL Multiphysics built-in water, while for the other materials, the parameters were inserted according to material datasheets and available literature. All data used in these simulations are shown in Table S4.

The fluid dynamics was analysed using the Navier–Stokes equation within the COMSOL Multiphysics Laminar Flow interface and the following assumptions were made according to the dynamics under analysis: the fluid was considered Newtonian and incompressible so that both density and viscosity could be assumed as constants. Furthermore, the no-slip boundary condition was applied on the exterior walls.[50] This setup is very common for studying these fluidic problems.[51–53] The fluid is considered confined in each well from the top so that all the free surface phenomena can be neglected. This approach is reasonable whenever the flow inside the wells can be considered laminar and under equilibrium. This allows to neglect all the transient phenomena (*e.g.* initial filling or fluid height changes inside the wells) and speed up the computation, by evaluating only a steady-state solution. The fluid was set to flow alongside the positive *x*-axis direction and different operating flow rates were evaluated, in particular: 50 μl min^{-1}, 100 μl min^{-1}, 200 μl min^{-1}, 300 μl min^{-1}, 400 μl min^{-1}, 500 μl min^{-1}. Through the Multiphysics node in COMSOL Multiphysics, the Laminar Flow interface was coupled with the Solid Mechanics one to capture the effect of the pressure of the fluid, on the

displacement and stress of the plate walls. This can be a very useful tool to predict failures in fluidic devices. Different domain probes were defined on the fluid volume for capturing the maximum velocity, maximum pressure on the walls and maximum displacement. For each domain, an independent, auto-generated and physics-based mesh was created. The elements of the mesh had a length between 0.9 mm and 5.3 mm. A mesh sensitivity study was developed using five different meshes and tested in the case of a constant flow rate of 50 μl min^{-1}. Each mesh had a different value for the maximum and minimum mesh element size. Fig. S3c–f show the maximum and minimum element sizes together with the results for the four parameters: maximum pressure, maximum velocity, maximum displacement and maximum stress. The data clearly confirm the stability of the results of the selected mesh.

To test simulations, experiments were performed using a two-head peristaltic pump (LiveFlow from IVTech), with the same flow rates tested with simulations. It was necessary to attach PDMS tubes with an inner diameter of 1 mm in the inlets and outlets of the plate using TEGORad 2800 photocrosslinked with a UV lamp. A 2% solution of ddH_2O and Disperse Blue (Aldrich Chemical Co) was used as flowing medium, collected in the reservoirs used as medium dispensing. The circuit was a loop flow, so each line of the BioFlowWellplate (*i.e.* three cascade wells connected by a channel) was equipped with only one reservoir, from which medium was injected in the circuit and in which medium from the circuit was discharged. The reservoirs contained a total of 10 ml of cell culture medium each and the length of each connection reservoir-BioFlowWellplate was 40 cm.

2.6. Cell culture

Cellular experiments were performed using Human keratinocytes (HaCaT) purched from Antibody Research Corporation, Human Fibroblast (HFF-1. Atcc), Endothelial cells (EC) kindly gifted by IRCCS Candiolo Institute and A549-GFP+ were kindly provided by Dr Valentina Monica, Department of Oncology, University of Torino, AOU San Luigi Gonzaga. HaCaT and HFF-1 were maintained in Gibco DMEM GlutaMAX high glucose supplemented with 15% Fetal Bovine Serum (Sigma Aldrich), 1% penicillin–streptomycin (Sigma Aldrich), 1% L-glutammine (Sigma Aldrich), 1% sodium pyruvate (Sigma Aldrich). EC were maintained in Gibco F12K supplemented with 10% Fetal Bovine Serum, 1% penicillin–streptomycin, 0.01 mg ml^{-1} Heparin (Sigma Aldrich) and brain extract supplement (Sigma Aldrich), while A549-GFP+ were cultured in Gibco BenchStable™ RPMI 1640 GlutaMAX medium supplemented with 10% Fetal Bovine Serum and 1% penicillin/streptomycin.

2.7. Conditioned medium

1×10^4 HaCaT, HFF-1, EC or A549 GFP+ cells were seeded onto a 96 well plate (TC treated, Greiner Bio-One) in complete medium (200 μL for each well) that was previously incubated with sterilized BioFlowWellplate (one device in 10 ml of medium, to be consistent with the protocol used in previous work[33]) for 72 h at 37 °C at 5% CO_2. The aim of this test is to evaluate the presence of any cytotoxic leachables (*e.g.*, residual monomers or photoinitiator derivatives) from the fabrication process. Cells were then cultured in humidified incubator at 37 °C in 5% CO_2 and after 24 h and 72 h MTT assay at the concentration of 0.5 mg ml^{-1} was used to evaluate the viability at each time point. After 2 h of incubation at 37 °C, the formazan salts were dissolved in 200 μl of DMSO and the absorbance at 570 nm (650 nm reference wavelength) was evaluated using Synergy™ HTX Fluorescence Multi-Mode Microplate Reader. The signal of the normal and conditioned medium without cells was used as background. The cell proliferation experiments were performed three times. Differences between groups were analyzed by two-way ANOVA.

2.8. Cell proliferation and immunostaining

1×10^4 A549 GFP+ cells were seeded onto a 96 well plate (TC treated, Greiner Bio-One) and the BioFlowWellplate, previously incubated for 30 min in gelatin type B (Sigma Aldrich) 0.15% w/v to enhance cell attachment, and cultured at 37 °C in 5% CO_2. After 24 h MTT assay was used as previously described to evaluate the difference in terms of cells seeding efficiency on the two substrates. Then, cells were cultured till 72 h and again MTT assay was used to analyse the proliferation rate on the two substrates. The cell proliferation experiments were performed three times. Differences between groups were analyzed by one or two-way ANOVA, depending on the variables.

To test for immunofluorescence, A549 GFP+ cells were seeded and, after 72 h of culture, were fixed with 4% paraformaldehyde (PFA, Sigma) at room temperature for 15 min and washed twice with PBS. For the staining, cells were permeabilized with 0.1 v/v% of Triton X-100 (Sigma-Aldrich) for 10 min and were then incubated with 0.4 μM DAPI in PBS and 11 μM Alexa Fluor Plus 555 phalloidin (Invitrogen) (200 μL) for 30 min at room temperature. The samples were imaged using the microscope Eclipse Ti2 Nikon (Tokyo, Japan) equipped with a Crest X-Light spinning disk. Three different fluorescent channels were evaluated: DAPI, FITC and TRITC lines.

2.9. Cell viability

To evaluate the ability of EC cells to attach to the Wellplate, propaedeutic for the following dynamic culture, 1×10^4 EC cells were seeded, previously incubated for 30 min in gelatin type B (Sigma Aldrich) 0.15% w/v to enhance cell attachment and cultured for 24 h at 37 °C in 5% CO_2. Then, LIVE/DEAD cell assay kit (Sigma-Aldrich) was used to evaluate cell viability and to obtain viability information. In detail, samples were stained with 1.5 μM propidium iodide (PI) and 1 μM Calcein-AM for 30 min in an incubator at 37 °C and then washed with DPBS to remove the unreacted dyes. The fluorescence signals were detected using the microscope Eclipse Ti2 Nikon (Tokyo, Japan) equipped with a Crest X-Light spinning disk.

2.10. Dynamic endothelium model

1×10^4 EC cells were seeded onto a standard 96 well plate (TC treated, Greiner Bio-One) and the BioFlowWellplate, previously incubated for 30 min in gelatin type B (Sigma Aldrich) 0.15% w/v to

enhance cell attachment and cultured for 2 h at 37 °C in 5% CO_2 to have cell attachment before the dynamic culture.

The BioFlowWellplate was then connected to a two-head peristaltic pump (LiveFlow from IVTech, reservoirs were obtained from the same manufacturer) and cultured under dynamic condition for 24 and 72 h at 37 °C in 5% CO_2 using a flow rate of 100 µl min^{-1}. Sterile conditions were maintained by placing the BioFlowWellplate inside a modified Petri allowing tube access. After each timepoint, cell proliferation was tested to compare commercial well plate and BioFlowWellplate under static conditions, as well as BioFlowWellplate in dynamic condition. Statistical analysis was performed usingtwo-way ANOVA.

2.11. GelMA scaffold preparation and dynamic test on 3D scaffold

Gelatin methacryloyl (GelMA) was produced, dissolved and sterilized as in previous works. In particular, formulations were obtained by dissolving GelMA (Degree of Functionalization based on Lys residues was 3.1%) at a concentration of 10% w/v in DMEM cell culture medium (gibco), previously combined with lithium phenyl-2,4,6-trimethylbenzoylphosphinate (LAP) as photoinitiator at a concentration of 2.5 mg ml^{-1}. The solutions were heated at 60 °C for 1 h and filtered through 0.45 µm and 0.22 µm PES membrane filters (Asimo) to sterilize.[44–48,54] GelMA solution was then pre-warmed at 37 °C before pouring in the BioFlowWellplate. To obtain a channel inside the scaffolds, a cannula needle with an external diameter of 0.8 mm and a length greater than the length of the Wellplate was incubated for 1 h at 37 °C with BSA (Sigma Aldrich) to prevent GelMA from attaching to the needle and inserted in one line of the Wellplate through the channels. Then, 300 µl of GelMA were poured in each well and photocrosslinked thanks to UV light irradiation (λ = 365 nm, Asiga® Flash Cure Box, I = 10 mW cm^{-2}) for 2 min. The cannula needle was then gently removed and PDMS tubes with an inner diameter of 1 mm were attached to the inlets and outlets of the plate using TEGORad 2800 photocrosslinked with a UV lamp. Dynamic perfusion of the scaffolds was conducted at 100 µl min^{-1} for various timepoints. Complete medium was used as flowing medium, dispensed in 15 ml in the reservoirs. The circuit was a loop flow, so each line was equipped with only one reservoir, from which medium was injected in the circuit but also in which medium from the circuit was discharged.

2.12. Statistical analysis

Experiments of cellular seeding efficiency and proliferation were conducted with three biological replicates, each of them with a technical triplicate and results are presented as the means ± standard deviation. The statistical analysis was conducted using two-way ANOVA through origin software, with p-values $^{*}P < 0.05$, $^{**}P < 0.01$, $^{***}P < 0.001$, $^{****}P < 0.0001$.

3. Results and discussion

3.1. 3D printed device

Building on previous studies that had already assessed the formulation and printing parameters for TEGORad printing,[33] specific modifications were implemented to enable fabrication of the bimaterial device. The composition of the PEGDA-based and TEGORad-based resins are reported in Tables S1 and S2, respectively, while Table S3 shows the updated exposure times applied to the different structural regions of the device. Fig. 1(a) presents the BioFlowWellplate, while the high resolution achieved is illustrated in Fig. 1(b). As detailed in Section 2.1, the well bottoms were engineered to be optically transparent; Fig. 1(c) confirms the successful fabrication of the transparent regions.

3.2. Fluidic simulations and tests

Within the simulated flow rate range, the domain probes values for what concerns the maximum fluid pressure, the maximum fluid velocity and the maximum displacement of the plate due to the pressure of the fluid on the walls and the average shear stress on the boundary surface between liquid and baseplate (crucial to investigate the behaviour of cells cultured under flow) are shown in Table S5.

To better visualize the fluid flow, the velocity field across the water domain and the pressure, in Fig. S4 are shown the

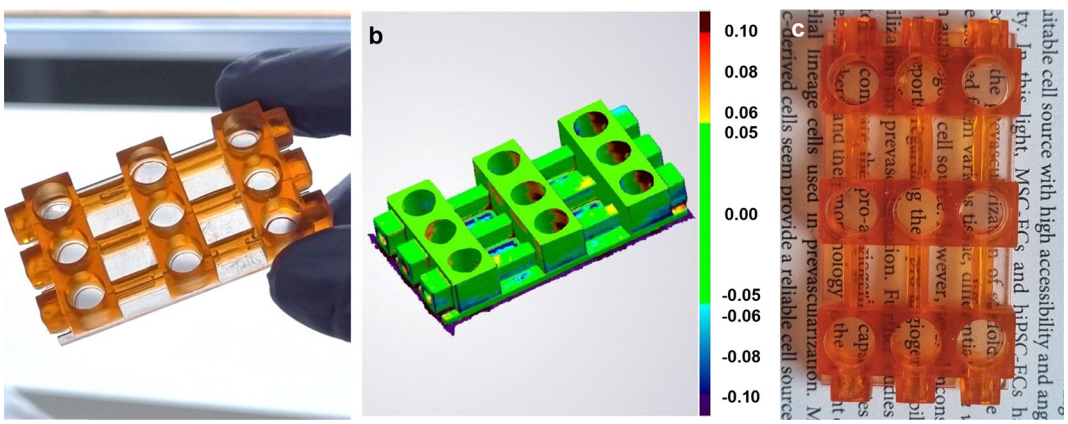

Fig. 1 (a) the BioFlowWellplate, (b) scanner 3D, (c) picture underlying bottom transparency.

streamline plots while in Fig. S5 the pressure plots for the different flow rates. As clearly visible, the water motion is very slow in the wells and the mixing capability increases as the flow rate grows. The maximum velocity is recorded in the channel between wells due to shrinking of cross section of the channel or at the ends of the channel both towards the inlet and the outlet. Furthermore, from Fig. S5, the major pressure drops are located at the channel ends on both sides while, within the wells, as confirmed by the velocity values in Fig. S4, the pressure is almost constant. As further evidence of that, the Von Mises stress is plotted in Fig. S6, alongside with the displacement, for a particular flow rate (f6 = 500 μl min^{-1}). The flow rate choice was made to confirm that even with the highest flow rate, the maximum stress (that is located at the bottom of the wells) stays well below the ultimate tensile strength of the material. In this case, the maximum stress recorded on the material is 1.1×10^3 N m^{-2}. This value is three orders of magnitude lower than the ultimate tensile strength of the involved materials, that is 4.5×10^6 N m^{-2} for PEGDA 250[55] and 0.7×10^6 N m^{-2} for TEGORad.[56] Looking at the streamlines (Fig. S4), for fluxes above 100 μl min^{-1} the turbulence in the first (but also the following) wells was high and the flux inhomogeneous. Moreover, for fluxes above 100 μl min^{-1}, pressures (Fig. S5) start to increase, in particular in the first well, A the upper part of the well has no constrains, a high pressure could lead to the filling and spillage of the culture medium. As predicted by simulations, for flow rates higher than 100 μl min^{-1}, the fluid starts to be turbulent and therefore the approximation of laminar flow under equilibrium does not apply any more, making weaker the steady-state solution. For these flow rates, the behaviour of the free surface of the fluid must be taken into account. Also the fluid height inside each well can potentially deviate one from another, even leading to some spillage phenomenon.

Once the simulations were carried out, tests were conducted directly on the plate. The selected pump (2-head peristaltic pump, LiveFlow, IVTech, Fig. 2(b)) allowed for testing the flows analysed through simulations. The tests had varying durations. The longest test lasted 10 days and demonstrated the maintenance of the steady-state flow condition both for 50 μl min^{-1} and for 100 μl min^{-1}, while quite immediate spillage from the first well was detected for the other flow rates. The experiments conducted underscored the feasibility of dynamic and automated cell culture. Fig. 2(a) shows BioFlowWellplate with the tubes polymerized in the inlets and outlets, while Fig. 2(b), the complete setup for tests is shown. The tubes and the reservoirs were autoclaved and their assembly with the BioFlowWellplate was performed under sterile conditions in a BLS-2 in sterility condition, biological hood. For the motivations illustrated, 100 μl min^{-1} flow rate was selected for following cellular experiments.

3.3. Microscopy feasibility

As will be discussed in Section 3.5, the low thickness and transparency of the wells bottom allow to monitor cells inside the wells. However, it is important to consider that BioFlowWellplate is 3D printed layer by layer from a PEGDA-based resin and therefore the images from the bottom are quite blurred. Consequently, those can give indications on the cellular colonization of the surface, but to have information on the morphology of the cells the microscopy has to be made from the top of the well. The fabricated platform has the great advantage to offer the possibility to easily detach the bottom part (where cells adhere) from the microfluidic compartment, using a simple blade. As shown in Fig. S7, starting from the 3D printed device (Fig. S7a) is possible to separate the bottom (Fig. S7b) and the upper (Fig. S7c) parts, with the former fits a microscopy glass slide (Fig. S7d), allowing and easy monitoring if the overall cellular conditions.

3.4. Conditioned medium

To gain an initial understanding of the possible cytotoxic effects of the materials used in BioFlowWellplate fabrication, we first performed conditioned medium (CM) assays. In these experiments, complete culture medium was incubated in the BioFlowWellplate for 72 hours under standard culture conditions. The medium was then collected and transferred to conventional culture plates containing epithelial HaCaT cells (Fig. 3(a)), HFF-1 fibroblasts (Fig. 3(b)), EC endothelial cells (Fig. 3(c)) or A549 GFP+ cells (Fig. 3(d)). Cytotoxicity tests were performed to identify any toxic compounds released by the device. The proliferation trends (Fig. 3) were highly promising,

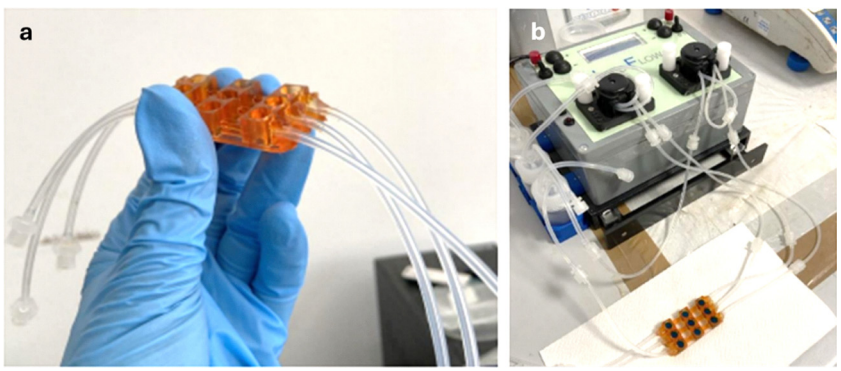

Fig. 2 (a) Cable connection by using UV lamp and (b) set up for tests.

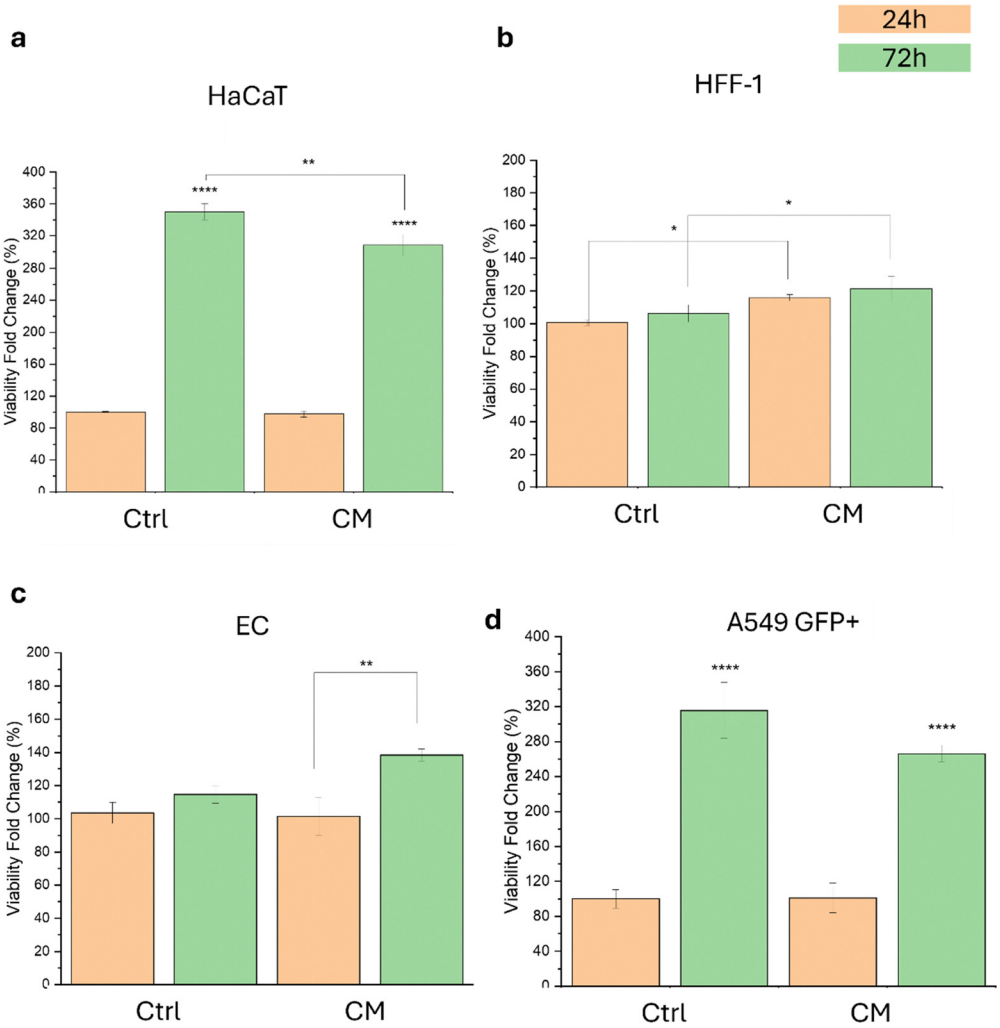

Fig. 3 Proliferation of (a) HaCaT, (b) HFF-1, (c) EC and (d) A549 GFP+ cell lines grown with BioFlowWellplate conditioned medium. Results are presented as the means ± standard deviation, normalized on the ctrl condition at 24 h. *$P < 0.05$, **$P < 0.01$, ***$P < 0.001$, ****$P < 0.0001$.

as no statistically significant cytotoxic effects were observed after 24 or 72 hours compared to the untreated control. From a biological point of view, this means that no cytotoxic compounds (*e.g.*, residual monomers, photoinitiator by-products, or other unreacted leachables) were released from the BioFlowWellplate. It should be noted that such analysis is of great importance when using the well plate to culture 3D cellularised scaffolds, as cytotoxic substances released from the material could penetrate the matrix and reduce cellular vitality. The absence of such substances suggests the feasibility of 3D cell culture experiments. From this point onwards, the next cellular experiments were conducted by seeding the cells directly into the wells of the BioFlowWellplate.

3.5. Cell seeding efficiency and growth and microscopy evaluation

Since BioFlowWellplate is fabricated to culture cells in dynamic conditions, next tests were performed on the cellular seeding efficiency and proliferation. A549 GFP+ were chosen in this case as they express Green Fluorescent Protein, useful for next fluorescence microscopy. The first evaluation concerned the cellular seeding efficiency (Fig. 4(a)). After 24, the metabolic activity of cells cultured was approximately half respect to the control (*i.e.* commercial polystyrene well plates). This first result was encouraging, considering that cells were attaching on a material different from polystyrene (that have been studied for cellular attachment since the '80s) without undergoing any surface functionalization.[57,58] Moreover, as reported in Fig. 4(b), after 72 h the growth rate of cells cultured on commercial polystyrene wells (ctrl) and BioFlowWellplate was the same (*i.e.* the metabolic activity was twice the one at 24 h). This means that, apart from an initial loss in terms of cellular seeding efficiency, explainable with the novelty of the material in cell culture, from a metabolic point of view cells then behaved in the same way of commercial polystyrene well plates, putting Wellplate in a prominent position for cellular tests and drug screening.

As the design aims was the feasibility for fluorescence microscopy, A549 GFP+ were cultured on both commercial polystyrene wells (ctrl) and the 3D printed device for 72 h and

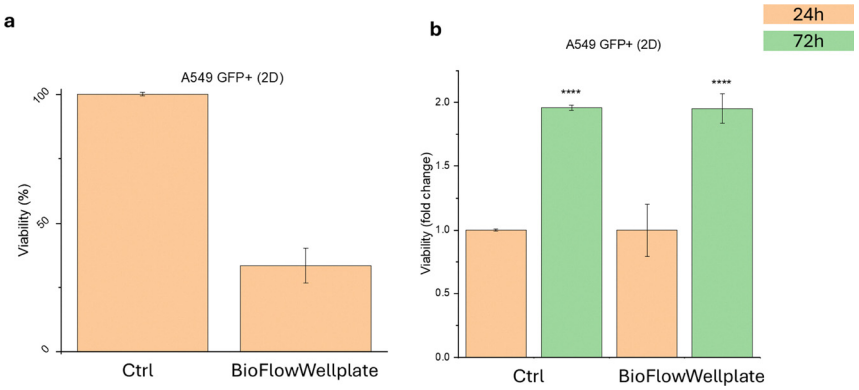

Fig. 4 (a) Cell seeding efficiency of A549 GFP+ cells after 24 h, expressed as viability normalized to cells cultured on standard polystyrene wells. (b) Proliferation of A549 GFP+ cells over 72 h on commercial polystyrene wells and the BioFlowWellplate, with each condition normalized to its own 24 h value to highlight relative growth rate. Results are presented as mean ± standard deviation. *$P < 0.05$, **$P < 0.01$, ***$P < 0.001$, ****$P < 0.0001$.

then fixed and stained with Alexa Fluor Plus 555 Phalloidin to be able to evaluate the possibility to analyse DAPI (Fig. 5 and Fig. S8a, e, i), FITC (Fig. 5 and Fig. S8b, f, j) and TRIC (Fig. 5 and Fig. S8c, g, k) channels. This cell line was chosen both because already put in contact with the presented materials[32,33] (but with different dye and different washing process) and also because expressing GFP they are a good option to test the material from an immunofluorescence point of view. Fig. 5 represents images collected with 4× objective, while Fig. S8 the 10× objective. Results showed that BioFlowWellplate allowed to monitor cellular colonization observing it from the bottom of the well (Fig. 5 and Fig. S8e–h), while to have more

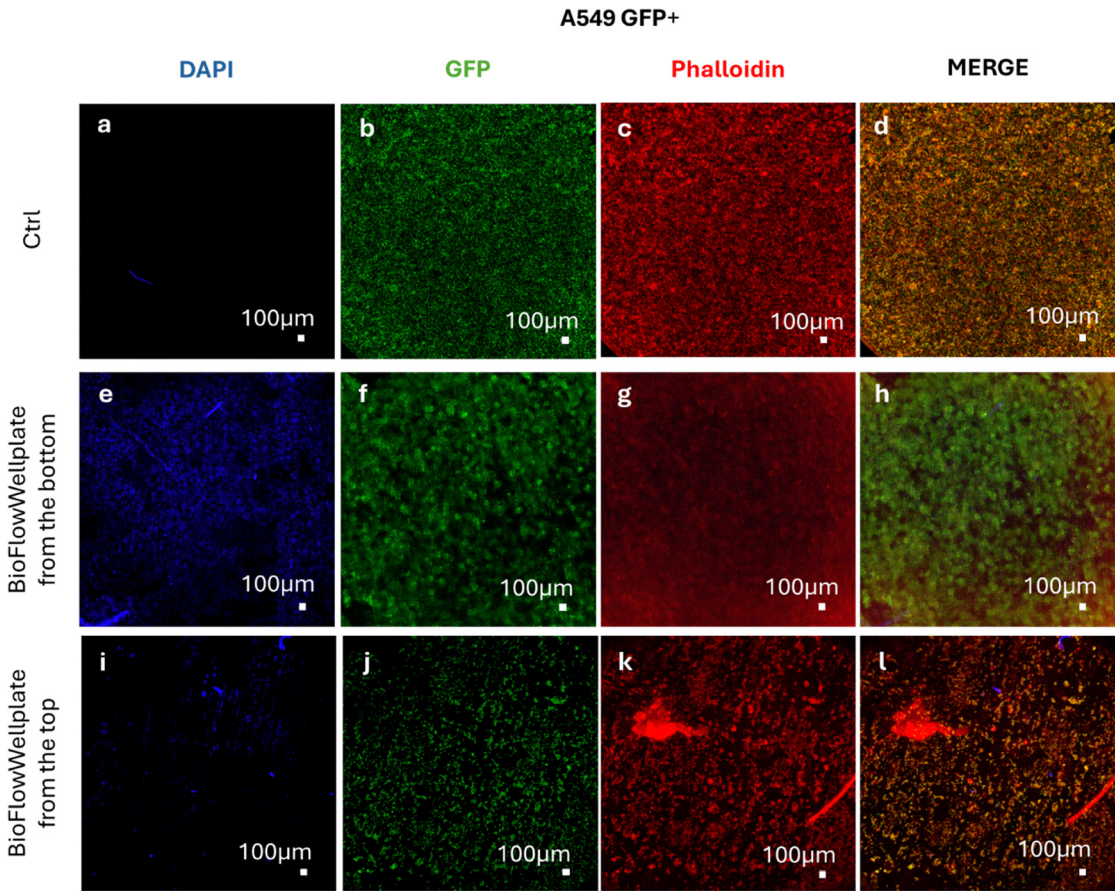

Fig. 5 A549 GFP+ colonization of commercial polystyrene wells (a)–(d) and of BioFlowWellplate wells, analysed both from the bottom of the well (e)–(h) and from the top of the well (i)–(l). Cells were stained with DAPI for the nuclei (blue, a, e, i) and Phalloidin for actin (red, c, g, k), while they already expressed GFP (green, b, f, j). Images were acquired at 4× magnification.

morphological information the detachment of the microfluidic compartment (Fig. S7) allowed to have more resolute microscopies (Fig. 5 and Fig. S8i–l). Moreover, confirming the results in Fig. 4, it was possible to observe a good cellular colonization of the well (Fig. 5 and Fig. S8e–l) respect to commercial polystyrene wells (Fig. 5 and Fig. S8a–d).

To note, the images in Fig. 5 were acquired at 4× magnification to provide an overall view of cell distribution. At lower magnification (4×), a slight reduction in DAPI signal contrast was observed in the BioFlowWellplate compared to polystyrene controls, likely due to the modest autofluorescence background of the 3D-printed PEGDA/TEGORad materials under this excitation. However, this effect was not detectable at higher magnifications (10×, Fig. S8), where the nuclei were clearly visible.

3.6. Live and dead

Preliminary to the dynamic culture of an endothelium model, EC cells attachment and survival for the first 24 h of culture was evaluated using LIVE/DEAD cell assay kit, staining living cells in green and dead cells in red. As shown shown in Fig. 6(b)–(f), EC easily attach in all the wells of the depicted line (*i.e.* three cascade wells connected through a channel) and the vitality of the cells was >98%, even if after 24 h the colonization was not already complete. However, the cell distribution appeared non-uniform, with a tendency to accumulate near the edges of the wells. This effect is attributed to a combination of the well geometry and the surface characteristics, which can influence initial cell sedimentation and adhesion under static conditions. To better understand this behavior, we performed a control experiment in which ECs were cultured for 24 hours on standard tissue culture treated polystyrene plates under identical conditions. The corresponding micrograph has been added to Fig. 6(a). On control plates, ECs exhibited a more homogeneous distribution, as expected for a surface optimized for cell adhesion. This comparison highlights the distinct cell–material interactions present in the 3D printed system and supports the need for dynamic culture to promote a more uniform colonization. Under dynamic conditions, fluid flow improves nutrient delivery and waste removal at the cell–material interface, reducing the local gradients that can occur in static culture. Moreover, the shear forces generated by flow help endothelial cells to spread more evenly across the surface, supporting the formation of a more homogeneous cell layer.

Despite partial coverage after 24 hours, the high viability and initial adhesion observed confirm that the BioFlowWellplate is suitable for hosting a dynamic endothelial model. It is important to note that Fig. 6 is intended to evaluate initial cell attachment and cytocompatibility. Proper vascularization experiments can be conducted using the device's microfluidic system, which allows controlled perfusion and the application of biochemical cues (*e.g.*, VEGF gradients) to guide endothelial sprouting and network formation. Additionally, the BioFlowWellplate is compatible with fluorescence imaging from both the bottom (Fig. 6(c) and (e)) and the top (Fig. 6(d) and (f)) of the wells, enabling detailed monitoring of cellular behavior throughout the device.

3.7. Dynamic endothelium model

After assessing the compatibility with the development of and endothelium model, primary EC were seeded on a 3D printed line and were allowe to adhere for 2 h. At this point the perfusion through peristaltic pump started with a flow rate of 100 μl min^{-1} (the setup is shown in Fig. 7(a) and (b)) and metabolic activity was analysed both after 24 and 72 h of culture (Fig. 7(c)). Results are shown compared to EC grown on commercial polystyrene wells (purple line at 100%). Results showed impressive improvement in cellular metabolic activity with dynamic culture, as after both 24 and 72 h it increased from less than 30% (static culture) to around 60% (dynamic culture) of the commercial polystyrene wells EC culture. This surge of the viability during the dynamic culture, recreated thanks both to the printed geometry and the set flow rate, indicated its promising potential for endothelium models culture, development and drug testing.

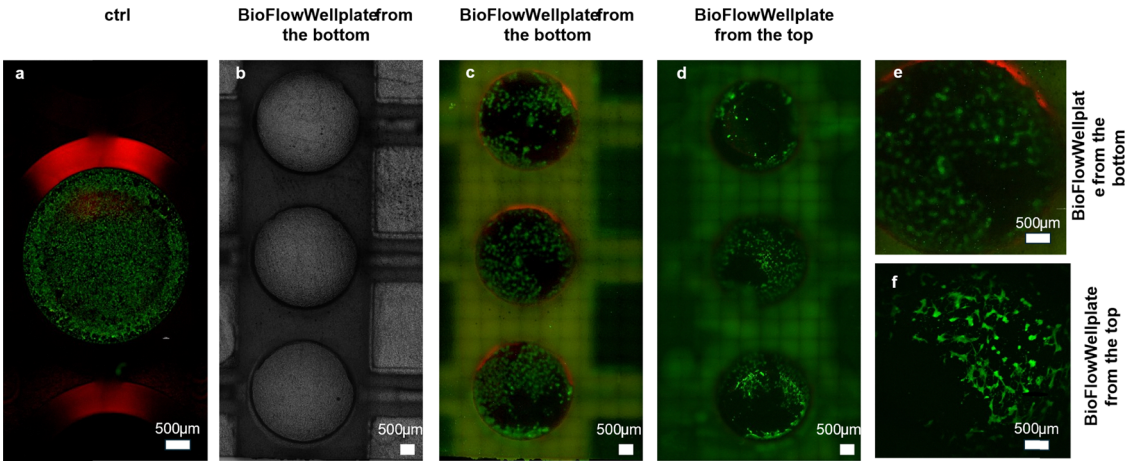

Fig. 6 Live and Dead assay for endothelial cells (EC) cultured on a tissue culture treated polystyrene plate (a), and a BioFlowWellplate line, analysed both from the bottom (b), (c), (e) and from the top (d), (f). Images were acquired at 4× in a 4 × 4 fields large image (a) 10 × 20 fields large image (b)–(d) and at 4× in (d) and (e).

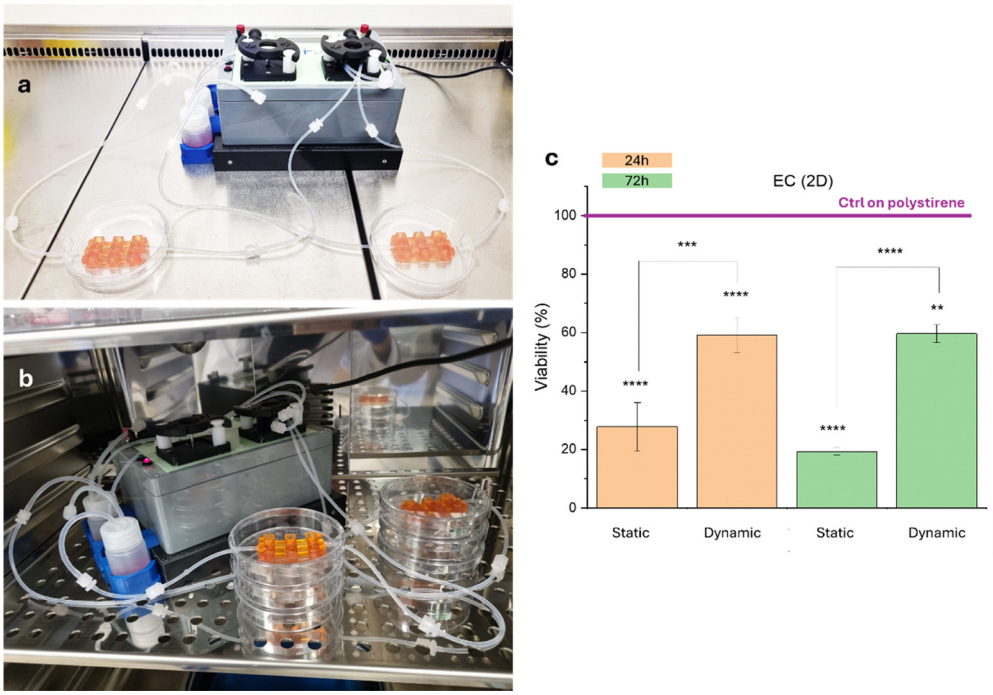

Fig. 7 Dynamic culture of the endothelium model: (a) the setup under a biological hood, (b) the setup in a biological incubator and (c) cellular viability in terms of metabolic activity respect to the control (*i.e.* commercial polystyrene wells).

3.8. 3D dynamic tests

At last, BioFlowWellplate was tested to perform dynamic culture of 3D scaffolds. GelMA was poured and photocrosslinked inside the wells, using a cannula needle to obtain the cavity, resembling a vessel through all the line (Fig. 8(a)). The medium used to visualize the flow and the medium diffusion a 1 : 50 solution of ddH_2O and Disperse Blue. (flow 100 μl min^{-1}, perfusion 24 h). As depicted in Fig. 8(b)–(e), the perfusion of 3D scaffolds was successful. Noteworthy, after 24 h the diffusion of the medium was high enough to spill out from the well (Fig. 8(e)). This highlights the need to colonize the vessel with endothelial cells to obtain an endothelium able to regulate the medium diffusion. In fact, it was already demonstrated that the diffusional permeability coefficient of vascular channels in 3D scaffold can be decreased by twofold if the channel has been seeded with endothelium when compared with that of a bare channel.[59] These first 3D perfusion tests together with the conditioned medium analysis in Section 3.4

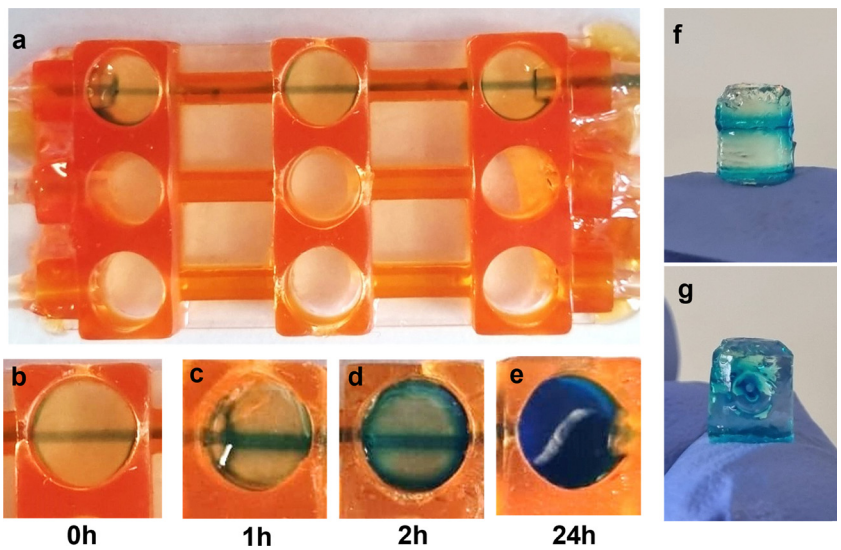

Fig. 8 Dynamic tests on 3D GelMA scaffold. (a) The perfused channel and magnification of the wells after (b) 0 h, (c) 1 h, (d) 2 h and (e) 24 h. (f) and (g) Represent the GelMA scaffold extracted from BioFlowWellplate.

demonstrated the feasibility of the 3D printed system also for the dynamic culture of 3D cellularized scaffolds. Future works will explore the development of a complex 3D *in vitro* model, cellularized and vascularized and its culture inside the platform, optimizing the BioFlowWellplate geometry for this purpose.

4. Conclusions

The presented work aimed to develop a 3D printed wellplate for the dynamic culture of *in vitro* models, with a design that can enable the testing using conventional instrumentation for cell culture analysis and monitoring. Therefore, it was designed to resemble the proportions of a 96-well commercial polystyrene well plate and equipped with a milled support to adapt it to various instrumentation. To take advantage of the excellent properties of both PEGDA 250 (great cytocompatibility, mechanical strength and transparency), and TEGORad® 2800 (great cytocompatibility, soft structure and low drug retention), a bimaterial device (BioFlowWellplate) was fabricated, using the former for the bottom part and the latter for the microfluidic. This device was successfully 3D printed employing DLP 3D printing.

For what concerns cellular compatibility, results were promising in terms of conditioned medium, cellular adhesion and proliferation, revealing the possibility to use this platform for more advanced applications. During the proliferation tests, it was also assessed the great suitability with fluorescence microscopy, both observing from the bottom of the plate, to have first indications of cellular colonization and overall conditions, and from the top, by easily removing the microfluidic part, to have information on cellular morphology.

Then, the 3D printed well plate was applied in the culture of a dynamic endothelium model, unveiling a great increment of endothelium metabolic activity when cultured in dynamic conditions. This endothelium model can be a powerful tool to study interactions between endothelium and drugs and treatments.

Finally, the support was tested for the dynamic perfusion of a 3D GelMA scaffold, evaluating the diffusion of the medium inside the scaffold, that highlight the need for endothelialisation of the vascular channel. This application represents a further step forward for these kinds of devices, since 3D *in vitro* models are nowadays gaining great interest in the field of tissues resembling and drug testing. Although the current work focused on fluidic validation and diffusion studies, preliminary results confirm that the BioFlowWellplate is suitable for 3D culture. Future work will include the seeding of endothelial and stromal cells within GelMA scaffolds under dynamic perfusion, to monitor cell viability and proliferation throughout the 3D matrix. Given the cytocompatibility of both PEGDA 250 and TEGORad® 2800 and the controlled perfusion conditions demonstrated here, the device provides a promising platform for supporting 3D cell growth and vascularization within soft hydrogels.

To conclude, the presented BioFlowWellplate showed good potential for 2D dynamic cell culture and 3D scaffold perfusion, and further studies will focus on enhancing the power of the device, overcoming the limitations analysed during the paper. In particular, it will be necessary to improve the initial cellular adhesion, studying cellular behaviour with different surface modifications. Then, efforts will be put on improving the microfluidic design to avoid spillage at higher flow rates. Lastly, the device design will be adapted for the culture of 3D *in vitro* models, enhancing the complexity of the systems in terms of number of cell types involved and studying the possibility to vascularize the channel to have physiologically relevant models to test drugs and therapies. On the other hand, being based on simple production methods and commercially available ingredient, this study can open interesting perspectives in for a wide range of application and offer valuable innovative research tools for biological studies.

Conflicts of interest

There are no conflicts to declare.

Data availability

The data supporting this article have been included as part of the supplementary information (SI). Supplementary information is available. See DOI: **https://doi.org/10.1039/d5tb01601k**.

Acknowledgements

This work was supported by the National Plan for Complementary Investments to the NRRP, project ''D34H—Digital Driven Diagnostics, prognostics and therapeutics for sustainable Health care'' (project code: PNC0000001), Spoke 4 funded by the Italian Ministry of University and Research. This work was supported by the National Recovery and Resilience Plan (NRRP), Mission 4 ''Education and Research'' – Component 2 ''From research to business'' – Investment 3.1 ''Fund for the realization of an integrated system of research and innovation infrastructures'' Call for tender no. 3264 of 28/12/2021 of Italian Ministry of Research funded by the European Union – Next Generation EU – Project code: IR0000027, Concession Decree no. 128 of 21/06/2022 adopted by the Italian Ministry of Research, CUP:B33C22000710006, Project title: iENTRANCE. This work has been co-funded by DM118/23 that received funding form NextGenerationEU.

References

1 Q. Zhang, L. Sito, M. Mao, J. He, Y. S. Zhang and X. Zhao, Current advances in skin-on-a-chip models for drug testing, *Microphysiol. Syst.*, 2018, **1**, 1, DOI: **10.21037/mps.2018.08.01**.

2 M. S. Kang, J. Jang, H. J. Jo, W. H. Kim, B. Kim, H. J. Chun, D. Lim and D. W. Han, Advances and Innovations of 3D Bioprinting Skin, *Biomolecules*, 2023, **13**, DOI: **10.3390/biom13010055**.

3 A. K. Jain, D. Singh, K. Dubey, R. Maurya, S. Mittal and A. K. Pandey, Models and Methods for *In Vitro* Toxicity, *In Vitro Toxicol*, Elsevier, 2018, pp. 45–65, DOI: 10.1016/B978-0-12-804667-8.00003-1.
4 *New Insights into Cell Culture Technology*, ed. S. J. T. Gowder, InTech, 2017, DOI: 10.5772/62590.
5 R. Rimal, Y. Marquardt, T. Nevolianis, S. Djeljadini, A. B. Marquez, S. Huth, D. N. Chigrin, M. Wessling, J. M. Baron, M. Möller and S. Singh, Dynamic flow enables long-term maintenance of 3-D vascularized human skin models, Appl, *Mater. Today*, 2021, **25**, DOI: 10.1016/j.apmt.2021.101213.
6 K. Kwapiszewska, A. Michalczuk, M. Rybka, R. Kwapiszewski and Z. Brzózka, A microfluidic-based platform for tumour spheroid culture, monitoring and drug screening, *Lab Chip*, 2014, **14**, 2096–2104, DOI: 10.1039/C4LC00291A.
7 P. Aishwarya, G. Agrawal, J. Sally and M. Ravi, Dynamic three-dimensional cell-culture systems for enhanced *in vitro* applications, *Curr. Sci.*, 2022, **122**, 149–160, DOI: 10.18520/cs/v122/i2/149-160.
8 D. Dupont and A. R. Mackie, Static and dynamic *in vitro* digestion models to study protein stability in the gastrointestinal tract, *Drug Discovery Today:Dis. Models*, 2015, **17–18**, 23–27, DOI: 10.1016/j.ddmod.2016.06.002.
9 S. Santaguida, D. Janigro, M. Hossain, E. Oby, E. Rapp and L. Cucullo, Side by side comparison between dynamic versus static models of blood–brain barrier *in vitro*: A permeability study, *Brain Res.*, 2006, **1109**, 1–13, DOI: 10.1016/j.brainres.2006.06.027.
10 B. D. Cardoso, E. M. S. Castanheira, S. Lanceros-Méndez and V. F. Cardoso, Recent Advances on Cell Culture Platforms for *In Vitro* Drug Screening and Cell Therapies: From Conventional to Microfluidic Strategies, *Adv. Healthcare Mater.*, 2023, **12**, DOI: 10.1002/adhm.202202936.
11 B. Zhang, A. Korolj, B. F. L. Lai and M. Radisic, Advances in organ-on-a-chip engineering, *Nat. Rev. Mater.*, 2018, **3**, 257–278, DOI: 10.1038/s41578-018-0034-7.
12 A. Chiadò, G. Palmara, A. Chiappone, C. Tanzanu, C. F. Pirri, I. Roppolo and F. Frascella, A modular 3D printed lab-on-a-chip for early cancer detection, *Lab Chip*, 2020, **20**, 665–674, DOI: 10.1039/c9lc01108k.
13 S. R. Meyer, C. J. Zhang, M. A. Garcia, M. C. Procario, S. Yoo, A. L. Jolly, S. Kim, J. Kim, K. Baek, R. D. Kersten, R. J. Fontana and J. Z. Sexton, A High-Throughput Microphysiological Liver Chip System to Model Drug-Induced Liver Injury Using Human Liver Organoids, *Gastro Hep Adv.*, 2024, **3**, 1045–1053, DOI: 10.1016/j.gastha.2024.08.004.
14 S. Rajasekar, D. S. Y. Lin, L. Abdul, A. Liu, A. Sotra, F. Zhang and B. Zhang, IFlowPlate—A Customized 384-Well Plate for the Culture of Perfusable Vascularized Colon Organoids, *Adv. Mater.*, 2020, **32**, DOI: 10.1002/adma.202002974.
15 J. Abello, S. Raghavan, Y. Y. Yien and A. N. Stratman, Peristaltic pumps adapted for laminar flow experiments enhance *in vitro* modeling of vascular cell behavior, *J. Biol. Chem.*, 2022, **298**, 102404, DOI: 10.1016/j.jbc.2022.102404.
16 C. Heuer, J. Preuß, T. Habib, A. Enders and J. Bahnemann, 3D printing in biotechnology—An insight into miniaturized and microfluidic systems for applications from cell culture to bioanalytics, *Eng. Life Sci.*, 2022, **22**, 744–759, DOI: 10.1002/elsc.202100081.
17 M. J. Lerman, J. Lembong, G. Gillen and J. P. Fisher, 3D printing in cell culture systems and medical applications, *Appl. Phys. Rev.*, 2018, **5**, DOI: 10.1063/1.5046087.
18 K. Ren, J. Zhou and H. Wu, Materials for microfluidic chip fabrication, *Acc. Chem. Res.*, 2013, **46**, 2396–2406, DOI: 10.1021/ar300314s.
19 M. Radisic and P. Loskill, Beyond PDMS and membranes: New materials for organ-on-a-chip devices, *ACS Biomater. Sci. Eng.*, 2021, **7**, 2861–2863, DOI: 10.1021/acsbiomaterials.1c00831.
20 G. Gonzalez, I. Roppolo, C. F. Pirri and A. Chiappone, Current and emerging trends in polymeric 3D printed microfluidic devices, *Addit. Manuf.*, 2022, **55**, 102867, DOI: 10.1016/j.addma.2022.102867.
21 G. M. Whitesides, The origins and the future of microfluidics, *Nature*, 2006, **442**, 368–373, DOI: 10.1038/nature05058.
22 I. D. Johnston, D. K. McCluskey, C. K. L. Tan and M. C. Tracey, Mechanical characterization of bulk Sylgard 184 for microfluidics and microengineering, *J. Micromech. Microeng.*, 2014, **24**, DOI: 10.1088/0960-1317/24/3/035017.
23 S. Halldorsson, E. Lucumi, R. Gómez-Sjöberg and R. M. T. Fleming, Advantages and challenges of microfluidic cell culture in polydimethylsiloxane devices, *Biosens. Bioelectron.*, 2015, **63**, 218–231, DOI: 10.1016/j.bios.2014.07.029.
24 S. Torino, B. Corrado, M. Iodice and G. Coppola, Pdms-based microfluidic devices for cell culture, *Inventions*, 2018, **3**, DOI: 10.3390/inventions3030065.
25 B. J. van Meer, H. de Vries, K. S. A. Firth, J. van Weerd, L. G. J. Tertoolen, H. B. J. Karperien, P. Jonkheijm, C. Denning, A. P. IJzerman and C. L. Mummery, Small molecule absorption by PDMS in the context of drug response bioassays, *Biochem. Biophys. Res. Commun.*, 2017, **482**, 323–328, DOI: 10.1016/j.bbrc.2016.11.062.
26 V. S. Shirure and S. C. George, Design considerations to minimize the impact of drug absorption in polymer-based organ-on-a-chip platforms, *Lab Chip*, 2017, **17**, 681–690, DOI: 10.1039/c6lc01401a.
27 M. W. Toepke and D. J. Beebe, PDMS absorption of small molecules and consequences in microfluidic applications, *Lab Chip*, 2006, **6**, 1484–1486, DOI: 10.1039/b612140c.
28 V. Ozbolat, M. Dey, B. Ayan, A. Povilianskas, M. C. Demirel and I. T. Ozbolat, 3D Printing of PDMS Improves Its Mechanical and Cell Adhesion Properties, *ACS Biomater. Sci. Eng.*, 2018, **4**, 682–693, DOI: 10.1021/acsbiomaterials.7b00646.
29 H. Zhang, T. Qi, X. Zhu, L. Zhou, Z. Li, Y. F. Zhang, W. Yang, J. Yang, Z. Peng, G. Zhang, F. Wang, P. Guo and H. Lan, 3D Printing of a PDMS Cylindrical Microlens Array with 100% Fill-Factor, *ACS Appl. Mater. Interfaces*, 2021, **13**, 36295–36306, DOI: 10.1021/acsami.1c08652.
30 C. Chen, B. T. Mehl, A. S. Munshi, A. D. Townsend, D. M. Spence and R. S. Martin, 3D-printed microfluidic devices: fabrication, advantages and limitations – a mini

review, *Anal. Methods*, 2016, **8**, 6005–6012, DOI: **10.1039/c6ay01671e**.

31 N. Bhattacharjee, C. Parra-Cabrera, Y. T. Kim, A. P. Kuo and A. Folch, Desktop-Stereolithography 3D-Printing of a Poly(dimethylsiloxane)-Based Material with Sylgard-184 Properties, *Adv. Mater.*, 2018, **30**, DOI: **10.1002/adma.201800001**.

32 G. González, D. Baruffaldi, C. Martinengo, A. Angelini, A. Chiappone, I. Roppolo, C. F. Pirri and F. Frascella, Materials testing for the development of biocompatible devices through vat-polymerization 3d printing, *Nanomaterials*, 2020, **10**, 1–13, DOI: **10.3390/nano10091788**.

33 S. Villata, M. Canta, D. Baruffaldi, A. Pavan, A. Chiappone, C. F. Pirri, F. Frascella and I. Roppolo, 3D printable acrylate polydimethylsiloxane resins for cell culture and drug testing, *Biomater. Sci.*, 2023, **11**, 2950–2959, DOI: **10.1039/D3BM00152K**.

34 N. Rahimi, Defenders and Challengers of Endothelial Barrier Function, *Front. Immunol.*, 2017, **8**, DOI: **10.3389/fimmu.2017.01847**.

35 A. B. Malik, J. J. Lynch and J. A. Cooper, Endothelial Barrier Function, *J. Invest. Dermatol.*, 1989, **93**, S62–S67, DOI: **10.1038/jid.1989.11**.

36 S. Muro, M. Koval and V. Muzykantov, Endothelial Endocytic Pathways: Gates for Vascular Drug Delivery, *Curr. Vasc. Pharmacol.*, 2004, **2**, 281–299, DOI: **10.2174/1570161043385736**.

37 L. Moroni, J. A. Burdick, C. Highley, S. J. Lee, Y. Morimoto, S. Takeuchi and J. J. Yoo, Biofabrication strategies for 3D *in vitro* models and regenerative medicine, *Nat. Rev. Mater.*, 2018, **3**, 21–37, DOI: **10.1038/s41578-018-0006-y**.

38 B. H. Lee, N. Lum, L. Y. Seow, P. Q. Lim and L. P. Tan, Synthesis and characterization of types A and B gelatin methacryloyl for bioink applications, *Materials*, 2016, **9**, DOI: **10.3390/ma9100797**.

39 C. Kilic Bektas and V. Hasirci, Cell loaded 3D bioprinted GelMA hydrogels for corneal stroma engineering, *Biomater. Sci.*, 2020, **8**, 438–449, DOI: **10.1039/c9bm01236b**.

40 I. Pepelanova, K. Kruppa, T. Scheper and A. Lavrentieva, Gelatin-methacryloyl (GelMA) hydrogels with defined degree of functionalization as a versatile toolkit for 3D cell culture and extrusion bioprinting, *Bioengineering*, 2018, **5**, DOI: **10.3390/bioengineering5030055**.

41 K. Yue, G. Trujillo-de Santiago, M. M. Alvarez, A. Tamayol, N. Annabi and A. Khademhosseini, Synthesis, properties, and biomedical applications of gelatin methacryloyl (GelMA) hydrogels, *Biomaterials*, 2015, **73**, 254–271, DOI: **10.1016/j.biomaterials.2015.08.045**.

42 X. Ma, C. Yu, P. Wang, W. Xu, X. Wan, C. S. E. Lai, J. Liu, A. Koroleva-Maharajh and S. Chen, Rapid 3D bioprinting of decellularized extracellular matrix with regionally varied mechanical properties and biomimetic microarchitecture, *Biomaterials*, 2018, **185**, 310–321, DOI: **10.1016/j.biomaterials.2018.09.026**.

43 C. G. Gaglio, D. Baruffaldi, C. F. Pirri, L. Napione and F. Frascella, GelMA synthesis and sources comparison for 3D multimaterial bioprinting, *Front. Bioeng. Biotechnol.*, 2024, **12**, DOI: **10.3389/fbioe.2024.1383010**.

44 S. Villata, M. Canta, D. Baruffaldi, I. Roppolo, C. F. Pirri and F. Frascella, 3D bioprinted GelMA platform for the production of lung tumor spheroids, *Bioprinting*, 2023, **36**, DOI: **10.1016/j.bprint.2023.e00310**.

45 S. Villata, F. Frascella, C. G. Gaglio, G. Nastasi, M. Petretta, C. F. Pirri and D. Baruffaldi, Self-standing gelatin-methacryloyl 3D structure using Carbopol-embedded printing, *J. Polym. Sci.*, 2024, **62**, 2259–2269, DOI: **10.1002/pol.20240037**.

46 M. Petretta, S. Villata, M. P. Scozzaro, L. Roseti, M. Favero, L. Napione, F. Frascella, C. F. Pirri, B. Grigolo and E. Olivotto, *In Vitro* Synovial Membrane 3D Model Developed by Volumetric Extrusion Bioprinting, *Appl. Sci.*, 2023, **13**, 1889, DOI: **10.3390/app13031889**.

47 S. Villata, D. Baruffaldi, R. Cue Lopez, C. Paoletti, P. Bosch, L. Napione, A. M. Giovannozzi, C. F. Pirri, E. Martinez-Campos and F. Frascella, Broadly Accessible 3D *In Vitro* Skin Model as a Comprehensive Platform for Antibacterial Therapy Screening, *ACS Appl. Mater. Interfaces*, 2024, DOI: **10.1021/acsami.4c16397**.

48 Y. Piao, H. You, T. Xu, H. P. Bei, I. Z. Piwko, Y. Y. Kwan and X. Zhao, Biomedical applications of gelatin methacryloyl hydrogels, *Eng. Regener.*, 2021, **2**, 47–56, DOI: **10.1016/j.engreg.2021.03.002**.

49 COMSOL AB, COMSOL Multiphysics® Reference Manual, (2024).

50 E. Lauga, M. Brenner and H. Stone, Microfluidics: The No-Slip Boundary Condition, *Springer Handbook of Experimental Fluid Mechanics*, Springer Berlin, Heidelberg, Berlin, Heidelberg, 2007, pp. 1219–1240, DOI: **10.1007/978-3-540-30299-5_19**.

51 L. Hyndman, S. McKee, N. J. Mottram, B. Singh, S. D. Webb and S. McGinty, Mathematical modelling of fluid flow and solute transport to define operating parameters for *in vitro* perfusion cell culture systems, *Interface Focus*, 2020, **10**, 20190045, DOI: **10.1098/rsfs.2019.0045**.

52 G. Mossotti, A. Piscitelli, F. Catania, M. Aronne, G. Galfré, A. Lamberti, S. Ferrero, L. Scaltrito and V. Bertana, Advances in Water Resource Management: An *In Situ* Sensor Solution for Monitoring High Concentrations of Chromium in the Electroplating Industry, *Water*, 2024, **16**, 1167, DOI: **10.3390/w16081167**.

53 J. Lee and A. B. Baker, Computational Analysis of Fluid Flow Within a Device for Applying Biaxial Strain to Cultured Cells, *J. Biomech. Eng.*, 2015, **137**, DOI: **10.1115/1.4029638**.

54 C. G. Gaglio, D. Baruffaldi, C. F. Pirri, L. Napione and F. Frascella, GelMA synthesis and sources comparison for 3D multimaterial bioprinting, *Front. Bioeng. Biotechnol.*, 2024, **12**, DOI: **10.3389/fbioe.2024.1383010**.

55 N. Rekowska, J. Huling, A. Brietzke, D. Arbeiter, T. Eickner, J. Konasch, A. Riess, R. Mau, H. Seitz, N. Grabow and M. Teske, Thermal, Mechanical and Biocompatibility Analyses of Photochemically Polymerized PEGDA250 for Photopolymerization-Based Manufacturing Processes,

Pharmaceutics, 2022, **14**, 628, DOI: **10.3390/pharmaceutics14030628**.

56 G. Gonzalez, A. Chiappone, K. Dietliker, C. F. Pirri and I. Roppolo, Fabrication and Functionalization of 3D Printed Polydimethylsiloxane-Based Microfluidic Devices Obtained through Digital Light Processing, *Adv. Mater. Technol.*, 2020, **5**, DOI: **10.1002/admt.202000374**.

57 A. S. Curtis, J. V. Forrester, C. McInnes and F. Lawrie, Adhesion of cells to polystyrene surfaces, *J. Cell Biol.*, 1983, **97**, 1500–1506, DOI: **10.1083/jcb.97.5.1500**.

58 S. Cai, C. Wu, W. Yang, W. Liang, H. Yu and L. Liu, Recent advance in surface modification for regulating cell adhesion and behaviors, *Nanotechnol. Rev.*, 2020, **9**, 971–989, DOI: **10.1515/ntrev-2020-0076**.

59 B. S. Kim, G. Gao, J. Y. Kim and D. W. Cho, 3D Cell Printing of Perfusable Vascularized Human Skin Equivalent Composed of Epidermis, Dermis, and Hypodermis for Better Structural Recapitulation of Native Skin, *Adv. Healthcare Mater.*, 2019, **8**, DOI: **10.1002/adhm.201801019**.